Characterization of a Fe/Y[subscript 2]O[subscript 3] metal/oxide interface using neutron and x-ray scattering

Citation: Watkins, E. B., A. Kashinath, P. Wang, J. K. Baldwin, J. Majewski, and M. J. Demkowicz. "Characterization of a Fe/Y[subscript 2]O[subscript 3] Metal/oxide Interface Using Neutron and x-Ray Scattering." Appl. Phys. Lett. 105, no. 4 (July 28, 2014): 041601. © 2014 AIP Publishing LLC

As Published: http://dx.doi.org/10.1063/1.4891432

Publisher: American Institute of Physics (AIP)

Persistent URL: http://hdl.handle.net/1721.1/94509

Version: Final published version: final published article, as it appeared in a journal, conference proceedings, or other formally published context

Characterization of a Fe/Y2O3 metal/oxide interface using neutron and x-ray scattering

E. B. Watkins, A. Kashinath, P. Wang, J. K. Baldwin, J. Majewski, and M. J. Demkowicz

Citation: Applied Physics Letters **105**, 041601 (2014); doi: 10.1063/1.4891432
View online: http://dx.doi.org/10.1063/1.4891432
View Table of Contents: http://scitation.aip.org/content/aip/journal/apl/105/4?ver=pdfcov
Published by the AIP Publishing

Characterization of a Fe/Y_2O_3 metal/oxide interface using neutron and x-ray scattering

E. B. Watkins,[1,a)] A. Kashinath,[2,3,a)] P. Wang,[1,4] J. K. Baldwin,[5] J. Majewski,[1,b)] and M. J. Demkowicz[2,b)]

[1]*Lujan Neutron Scattering Center, Los Alamos National Laboratory, Los Alamos, New Mexico 87545, USA*
[2]*Department of Materials Science and Engineering, Massachusetts Institute of Technology, Cambridge, Massachusetts 02139, USA*
[3]*Computational Modeling Technology, Aramco Research Center—Boston, Cambridge, Massachusetts 02139, USA*
[4]*Intel Corporation, Hillsboro, Oregon, 97006, USA*
[5]*Center for Integrated Nanotechnologies, Los Alamos National Laboratory, Los Alamos, New Mexico 87545, USA*

(Received 29 May 2014; accepted 15 July 2014; published online 28 July 2014)

The structure of metal/oxide interfaces is important to the radiation resistance of oxide dispersion-strengthened steels. We find evidence of gradual variations in stoichiometry and magnetization across a Fe/Y_2O_3 metal/oxide heterophase interface using neutron and x-ray reflectometry. These findings suggest that the Fe/Y_2O_3 interface is a transitional zone approximately ~64 Å-thick containing mixtures or compounds of Fe, Y, and O. Our results illustrate the complex chemical and magnetic nature of Fe/oxide interfaces and demonstrate the utility of combined neutron and x-ray techniques as tools for characterizing them. © *2014 AIP Publishing LLC*.
[http://dx.doi.org/10.1063/1.4891432]

Nanoscale Y-Ti-O oxide precipitates are thought to play a major role in the radiation resistance of oxide dispersion-strengthened (ODS) steels.[1] In particular, the interfaces between these particles and the ferritic matrix are presumed to be excellent sinks for impurities created during nuclear reactions, such as helium (He^{2+}).[2] Improved models of the structure of these interfaces would be helpful in understanding and, eventually, improving the radiation resistance of ODS steels. However, due to the mixed ionic/covalent/metallic bonding present at metal/oxide interfaces, their structure is generally much more complex and difficult to investigate than that of metal/metal[3] or even oxide/oxide[4] interfaces. Moreover, according to Gibbs' phase rule, equilibrium phases absent from phase diagrams of bulk materials may, nevertheless, be found at metal/oxide interfaces, given the number of chemical species that meet there.[5,6]

We present an experimental investigation of the local structure of a Fe/Y_2O_3 metal/oxide heterophase interface using a combination of neutron (NR) and x-ray (XR) reflectometry as well as x-ray diffraction (XRD). This interface involves only three elements and its oxide component has a well-defined stoichiometry. Fe/Y_2O_3 is therefore easier to investigate than the more complex Fe/Y-Ti-O interfaces found in ODS steels[1,2] and can serve as a useful model system for understanding the influence of interfacial bonding on local interface structure. Our investigation reveals gradual variations in stoichiometry and magnetization across a ~64 Å-thick transition zone at this interface, demonstrating that its structure differs markedly from the neighboring bulk phases.

Complementary NR and XR techniques may be used to study the structure of thin films as a function of depth with near Å-level resolution.[7] NR is sensitive to density, chemical composition, and magnetization. XR is also sensitive to density and composition, but with different scattering contrast than NR (electronic *vs.* nuclear), and is almost insensitive to magnetic structure. Unlike analytical transmission electron microscopy (TEM)[8] or atom probe tomography (APT),[9] which are also capable of Å-level characterization of interface composition, NR and XR are non-destructive and do not suffer from artifacts that may arise from the proximity of free surfaces or sample preparation. However, they require flat samples of relatively large surface area (~50–500 mm^2) and high-perfection, i.e., uniform layer thickness, density, and composition as well as low surface roughness.

We use room temperature RF magnetron sputtering to grow high-quality α-Fe and Y_2O_3 films on Si (100) substrates with a 1 μm-thick SiO_2 surface oxide. For Fe deposition, using 2 mTorr, 400 watt DC, and 30 SCCM of Ar flow results in a growth rate of 0.37 nm/s. To grow Y_2O_3, we use a Y_2O_3 target at a process pressure of 5 mTorr, RF power of 200 watt, and an Ar flow of 30 SCCM, yielding a deposition rate of 0.012 nm/s. The base pressure of the deposition chamber is $<5.0 \times 10^{-8}$ Torr. Two samples are synthesized: A nominally 40 nm-thick layer of monolithic Y_2O_3 and a bilayer of Fe and Y_2O_3, each layer being nominally 20 nm thick with the Fe layer adjacent to the SiO_2 surface. The latter sample contains one Fe/Y_2O_3 interface.

We perform NR measurements using the Surface Profile Analysis Reflectometer (SPEAR) at the Lujan Neutron Scattering Center at Los Alamos National Laboratory.[10] The neutron beam is obtained from a spallation source and moderated by liquid H_2. In the experiment, neutrons impinge on a sample at a small angle, θ, and the ratio of elastically scattered to incident neutrons is measured. This ratio is defined

[a)]E. B. Watkins and A. Kashinath contributed equally to this work.
[b)]Authors to whom correspondence should be addressed. Electronic mail: demkowicz@mit.edu and jarek@lanl.gov

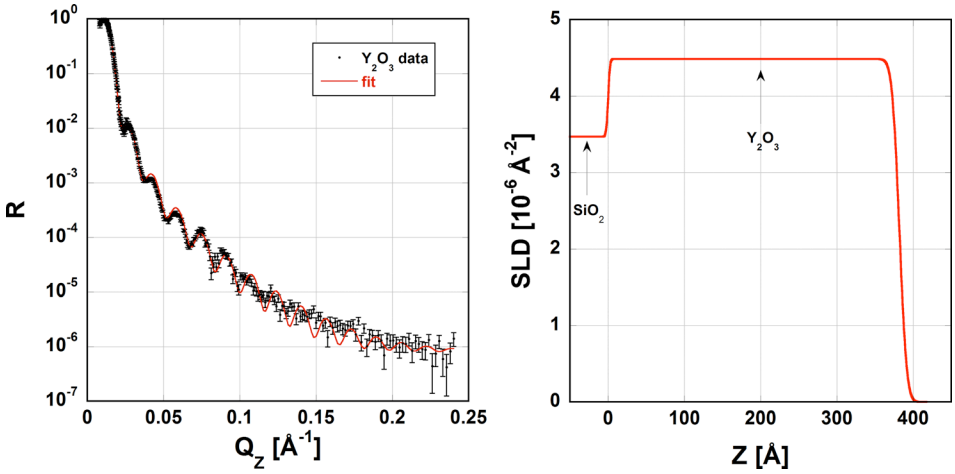

FIG. 1. (*left*) NR data (circles) from the Y_2O_3 monolayer and fitted reflectivity (solid red line). Error bars in the data show the statistical uncertainty of the measurement. (*right*) n-SLD profile from which the NR fit is obtained. The interface with the SiO_2 substrate is at $z = 0$.

as the reflectivity, R, and measured as a function of the momentum transfer vector, Q_z, where $Q_z = 4\pi\sin(\theta)/\lambda$. In a time-of-flight (ToF) instrument such as SPEAR, neutron momentum—and therefore wavelength, λ—may be determined by measuring the angle of scattered neutrons and the time it takes the neutrons to travel the length of the instrument. Neutron wavelengths at SPEAR range from 4.5 to 16 Å. To cover the range $0.001 < Q_z < 0.25\ \text{Å}^{-1}$, measurements are performed at three different incident angles: $\theta = \sim 0.5$, ~ 1.0, ~ 2.6 degrees. XR and XRD are performed using a θ–2θ Rigaku Ultima III x-ray diffractometer with Goebel mirror and a set of footprint limiting slits and in Bragg-Brentano geometry, respectively. We used a 2 kW linear x-ray source with Cu K_α radiation ($\lambda = 1.5418$ Å) and a curved graphite monochromator.

Analysis of specular NR data provides information on the coherent nuclear scattering length density (n-SLD) and the magnetic component of the scattering length density (m-SLD)[11] as a function of depth normal to the sample surface. The n-SLD depth profile is uniquely determined by the composition and density of the sample and m-SLD by the magnetic properties of the film. Because the SPEAR neutron beam is not polarized, reflectivities for spin-up and spin-down polarizations in magnetic films are added incoherently to simulate the measured reflectivity curve. This procedure assumes that magnetic domains are larger than the coherency of the neutron beam ($\sim\mu$m). XR provides information on the x-ray scattering length densities (x-SLD), which are generally complex to account for x-ray absorption.

The Y_2O_3 monolayer and Fe/Y_2O_3 bilayer are approximated by layered slab models parameterized by layer thickness, n-SLD, m-SLD (in the case of Fe), x-SLD, and interface roughness. The models consist of oxide and metal layers sandwiched between a super-phase (air) and a sub-phase (SiO_2). We use tabulated bound coherent scattering length (BCSL) values[12] for Si, Y, O, and Fe in the model. Given a trial SLD profile, the Abeles matrix method[13] as implemented in Motofit[14] and the Parratt formalism employed in locally developed fitting programs[15] are used to calculate the corresponding reflectivity curves. The model is then refined to optimize the χ^2 goodness of fit[16] between the calculated and measured reflectivity curves by changing the parameters describing each layer. To avoid over-parameterization, structural models employing the minimum number of layers to yield satisfactory fits are used.[15]

NR curves for the Y_2O_3 monolayer are shown in Fig. 1(*left*) and the model parameters for the best-fit SLD profile, plotted in Fig. 1(*right*), are given in Table I. There is good agreement between the measured and calculated NR corresponding to the fitted n-SLD profile. The fitted SLD is constant throughout the depth of the layer, consistent with stoichiometric Y_2O_3 of uniform density. The increased roughness of the Y_2O_3 free surface compared to the interface with the SiO_2 substrate is likely due to the columnar microstructure of the Y_2O_3, which has lower overall thickness near column boundaries than in column centers due to grain boundary grooving at the surface. This result confirms that the Y_2O_3 depositions, NR measurements, and reflectivity modeling methods are reliable.

NR curves for the Fe/Y_2O_3 bilayer are shown in Fig. 2 (*left*), and the model parameters for the best-fit SLD profile, plotted in Fig. 2 (*right*), are given in Table II. Agreement between the NR measurement and calculated reflectivity from the best-fit SLD profile is very good. The NR data may only be fitted if neutron scattering due to spontaneous magnetization of the Fe layer is taken into account. The combined (nuclear and magnetic) SLD profiles obtained from the NR fit are shown in Fig. 2(*right*). The red and blue solid curves represent the SLD profiles obtained for incoming neutrons in spin-up and spin-down states, respectively. In the first case, the m-SLD of $5.3 \times 10^{-6}\ \text{Å}^{-2}$ is added to the n-SLD while in the second case it is subtracted. Reflectivities for spin-up and spin-down neutron polarizations as well as their equally weighted average are shown in Fig. 2(*left*). The XR fit is shown in Fig. 3, and the associated model parameters are presented in Table III.

TABLE I. Model parameters used to fit NR data for Y_2O_3 on a SiO_2 substrate.

Layer	Thickness (Å)	n-SLD (10^{-6} Å^{-2})	Roughness (Å)
SiO_2	…	3.47[a]	2
Y_2O_3	382.1 ± 2	4.48	7.6

[a]parameters constrained to the theoretical values.

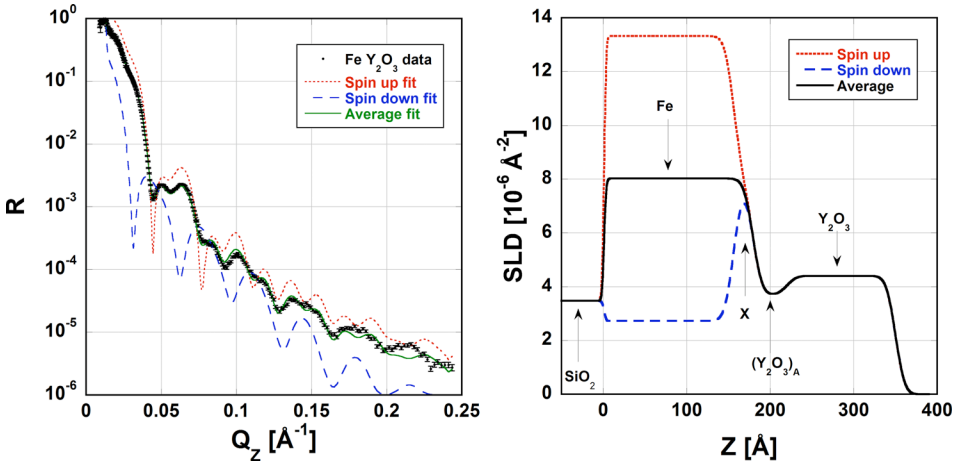

FIG. 2. (*left*) NR data (circles) from the Fe/Y_2O_3 bilayer, fitted total reflectivity (solid green line), and fitted partial reflectivities for spin-up and spin-down beam polarizations (dashed red and blue lines, respectively). Error bars in the data show the statistical uncertainty of the measurement. (*right*) n-SLD profile from which the NR fit is obtained. The SLD of the Fe layer has different m-SLD contributions for the spin-up and spin-down components of the beam (red and blue lines, respectively). The interface with the SiO_2 substrate is at $z = 0$.

TABLE II. Model parameters used to fit NR data for Fe/Y_2O_3 on a SiO_2 substrate. The m-SLD of 5.3×10^{-6} Å^{-2} was only applied to the Fe layer.[15]

Layer	Thickness (Å)	n-SLD (10^{-6} Å^{-2})	Roughness (Å)
SiO_2	…	3.47[a]	2 ± 0.5
Fe	155.4 ± 2	8.02[a]	8.8 ± 0.5[b]
X	22.8 ± 2	8.02 ± 0.2	8.8 ± 0.5[b]
$(Y_2O_3)_A$	41.0 ± 2	3.70 ± 0.2	8.8 ± 0.5[b]
Y_2O_3	129.7 ± 2	4.40[a]	8.8 ± 0.5[b]

[a]parameters constrained to the theoretical values.
[b]parameters constrained to be equal.

Aside from the Fe/Y_2O_3 interface, both the n-SLD and m-SLD distributions in Fig. 2 (*right*) as well as the x-SLD in Fig. 3 (right) match the expected values for Fe and fully dense, stoichiometric Y_2O_3. However, n-SLDs and x-SLDs immediately adjacent to the Fe/Y_2O_3 interface deviate markedly from those of Y_2O_3 and Fe. Adjacent to the 155.4 Å-thick Fe layer (measured from the SiO_2 interface), there is a 22.8 Å non-magnetic layer, labeled X. This region is especially visible in the spin-down (blue) SLD curve. Layer X is followed by a region 41 Å thick labeled $(Y_2O_3)_A$ with SLDs just below that of fully dense, stoichiometric Y_2O_3.

The lower than bulk Y_2O_3 SLD of the $(Y_2O_3)_A$ layer cannot be explained by Fe substitution of the Y sites because BCSL values of the elements at this interface increase as O < Y < Fe.[12] Furthermore, because of the high formation energies of antisite defects in Y_2O_3,[17] it is not likely that the SLD is due to Y substitution on O sites. The SLD of $(Y_2O_3)_A$ layer may be explained by Y or O vacancies or by lowered density compared to the bulk material, possibly due to porosity. For example, the difference in n-SLD between $(Y_2O_3)_A$ and Y_2O_3 may be accounted for by a ~15% decrease in the density of this layer or similar deficiency of the number of either Y or O atoms. Layer X has an n-SLD close to that of Fe, but is not magnetic. Meanwhile, its x-SLD is close to that of Y_2O_3. One possible interpretation of these results is to identify layer X as consisting of Fe_2O_3, with n-SLD of 7.2×10^{-6} Å^{-2} and x-SLD of 4.1×10^{-5} Å^{-2}. Fe_2O_3 exhibits several phases with different magnetic properties.[18]

Fig. 4 shows the XRD 2θ region from 10° to 60°. Using the Powder Diffraction Inorganic Crystal Structure Databases,[19] four crystallographic reflections may be identified. Peak (1) corresponds to amorphous SiO_2, (2) is the (002) peak of Y_2O_3, and (4) the (110) peak of Fe. These peaks are consistent with the epitaxial texture in the Fe/Y_2O_3 bilayer.[11] This well-defined epitaxial relation suggests that the Fe/Y_2O_3 interface is initially atomically sharp upon deposition and subsequently reacts to form the wide, transitional zone described here.

Peak (3) in Fig. 4 may be indexed as a (104) x-ray reflection from Fe_2O_3, in agreement with the inference made from NR and XR data. However, several more complex scenarios may also be consistent with the marked composition

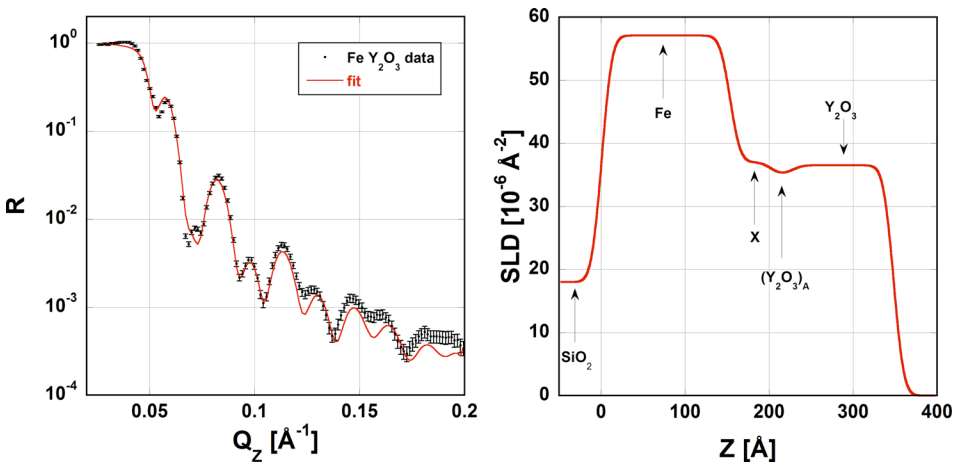

FIG. 3. (*left*) XR data (circles) from the Fe/Y_2O_3 bilayer and fitted reflectivity (solid red line). Error bars in the data show the statistical uncertainty of the measurement. (*right*) x-SLD profile from which the XR fit is obtained. The interface with the SiO_2 substrate is at $z = 0$.

TABLE III. Model parameters used to fit XR data for Fe/Y_2O_3 on a SiO_2 substrate.

Layer	Thickness (Å)	x-SLD (10^{-6} Å^{-2})	Roughness (Å)
SiO_2	…	18.0[a]	2[b]
Fe	153.8 ± 2	56.5[a]	8.8[b]
X	22.8 ± 2	37.0 ± 0.2[c]	8.8[b]
$(Y_2O_3)_A$	41.0 ± 2	35.0 ± 0.2[c]	8.8[b]
Y_2O_3	129.1 ± 2	37.1[a]	8.8[b]

[a]parameters allowed to vary ±5% from their theoretical values.
[b]parameters fixed to the values obtained from NR fits (Table II).
[c]parameters allowed to vary ±10% from their theoretical values.

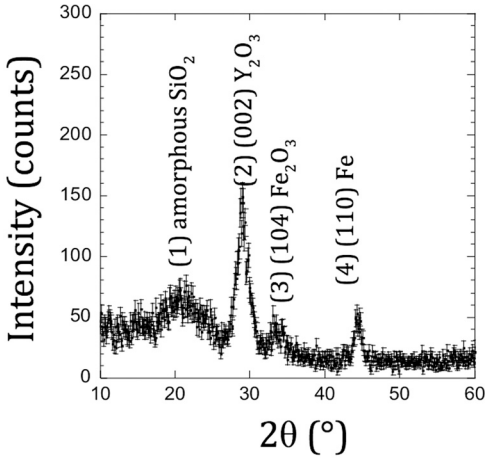

FIG. 4. XRD data from the Fe/Y_2O_3 bilayer on SiO_2 substrate. Error bars represent the statistical uncertainty of the measurement.

changes occurring at the Fe/Y_2O_3 interface, including roughening, mixing, or formation of ternary compounds. The Y-Fe-O system exhibits at least three such compounds:[20] $Y_3Fe_5O_{12}$, $YFeO_3$, and YFe_2O_4. Distinctive interfacial phases or "complexions" may also form.[6] Differences in stoichiometry at metal/oxide interfaces may be driven by bulk thermodynamics[20] as well as by the local interfacial environment.[6]

Our study reveals a 63.8 Å-thick (41 Å + 22.8 Å) region at the Fe/Y_2O_3 interface that differs from Y_2O_3 and Fe in composition, density, and magnetization. By contrast, previous NR investigations did not reveal such differences in impurity-free metal/metal heterophase interfaces.[21] Changes in structure and stoichiometry such as those observed here may also be expected at interfaces between Y-Ti-O oxide particles and the ferritic matrix in ODS steels. Such changes may play a role in explaining the local enhancement of Ti, Cr, or V at these interfaces.[22] Given that interfacial regions with altered stoichiometry, density, and magnetization may be as thick as ~64 Å, oxide particles with diameters below ~10 nm in ODS steels may be expected to exhibit markedly different structure and properties from bulk Y-Ti-O.

Our work demonstrates the utility of combining NR, XR, and XRD for investigating buried metal/oxide interfaces, similar to those found in ODS steels. NR investigations of Fe/Y-Ti-O metal/oxide interfaces with compositions closer to those in ODS steels may be performed in the future, provided that high-perfection samples of sufficiently large area may be synthesized. By combining NR with TEM and APT characterization, a more complete understanding of metal/oxide interfaces may be obtained.

This work was supported by the Laboratory Directed Research and Development (LDRD) program at Los Alamos National Laboratory under Project No. 20130118DR, under DOE Contract No. DE-AC52-06NA25396. This work also benefited from the use of the Lujan Neutron Scattering Center at LANSCE, funded by the DOE Office of Basic Energy Sciences and Los Alamos National Laboratory under DOE Contract No. DE-AC52-06NA25396. We are grateful to O. Anderoglu, B. P. Uberuaga, S. Yadav, M. Fitzsimmons, and S. Choudhury for helpful discussions and L. Daemen and D. Williams for assistance with x-ray measurements.

[1]M. J. Demkowicz, P. Bellon, and B. D. Wirth, MRS Bull. **35**(12), 992 (2010).
[2]G. R. Odette and D. T. Hoelzer, JOM **62**(9), 84 (2010); G. R. Odette, M. J. Alinger, and B. D. Wirth, Annu. Rev. Mater. Res. **38**(1), 471 (2008); P. Erhart, J. Appl. Phys. **111**(11), 113502 (2012).
[3]M. J. Demkowicz, J. Wang, and R. G. Hoagland, in *Dislocations in Solids*, edited by J. P. Hirth (Elsevier, Amsterdam, 2008), Vol. 14, p. 141; A. Kashinath, A. Misra, and M. J. Demkowicz, Phys. Rev. Lett. 110(8), 086101 (2013).
[4]M. J. Zhuo, B. P. Uberuaga, L. Yan, E. G. Fu, R. M. Dickerson, Y. Q. Wang, A. Misra, M. Nastasi, and Q. X. Jia, J. Nucl. Mater. **429**, 177 (2012).
[5]F. Ernst, Mater. Sci. Eng., R **14**(3), 97 (1995).
[6]P. R. Cantwell, M. Tang, S. J. Dillon, J. Luo, G. S. Rohrer, and M. P. Harmer, Acta Mater. **62**, 1 (2014).
[7]H. Zabel, Appl. Phys. A **58**(3), 159 (1994).
[8]C. Colliex, L. Bocher, F. de la Pena, A. Gloter, K. March, and M. Walls, JOM **62**(12), 53 (2010).
[9]G. Schmitz, C. Ene, H. Galinski, R. Schlesiger, and P. Stender, JOM **62**(12), 58 (2010).
[10]M. Dubey, M. S. Jablin, P. Wang, M. Mocko, and J. Majewski, Eur. Phys. J. Plus **126**(11), 11110 (2011).
[11]In *Modern Techniques for Characterizing Magnetic Materials*, edited by Yimei Zhu (Springer US, 2005), pp. 107.
[12]V. F. Sears, Neutron News **3**(3), 26 (1992).
[13]O. S. Heavens, *Optical Properties of Thin Solid Films* (Dover Publications, New York, 1991), p. 7; F. Abeles, J. Phys. Radium **11**(7), 307 (1950).
[14]A. Nelson, J. Appl. Crystallogr. **39**, 273 (2006).
[15]See supplementary material at http://dx.doi.org/10.1063/1.4891432 for a description of how the magnetic component of the SLD was fitted as well as of how the number of layers in the model was selected.
[16]C. B. Markwardt, Astron. Soc. P **411**, 251 (2009); K. Pearson, Philos. Mag. **50**(302), 157 (1900).
[17]J. X. Zheng, G. Ceder, T. Maxisch, W. K. Chim, and W. K. Choi, Phys. Rev. B **73**(10), 104101 (2006).
[18]R. S. Tebble and D. J. Craik, *Magnetic Materials* (Wiley-Interscience, 1969).
[19]G. J. Mccarthy, A. D. Mighell, C. R. Hubbard, and M. C. Nichols, Acta Crystallogr. A **40**, C442 (1984).
[20]K. Kitayama, M. Sakaguchi, Y. Takahara, H. Endo, and H. Ueki, J. Solid State Chem. **177**(6), 1933 (2004); V. Raghavan, *Phase Diagrams of Ternary Iron Alloys* (ASM International, 1987); K. T. Jacob and G. Rajitha, Solid State Ionics **224**, 32 (2012).
[21]M. Zhernenkov, M. S. Jablin, A. Misra, M. Nastasi, Y.-Q. Wang, M. J. Demkowicz, J. K. Baldwin, and J. Majewski, Appl. Phys. Lett. **98**, 241913 (2011); A. Kashinath, P. Wang, J. Majewski, J. K. Baldwin, Y. Q. Wang, and M. J. Demkowicz, J. Appl. Phys. **114**(4), 043505 (2013).
[22]E. A. Marquis, Appl. Phys. Lett. **93**(18), 181904 (2008).